Automated 3D Lumbar Intervertebral Disc Segmentation from MRI Data Sets

Xiao Dong and Guoyan Zheng

Abstract This paper proposed an automated 3D lumbar intervertebral disc (IVD) segmentation strategy from MRI data. Starting from two user supplied landmarks, the geometrical parameters of all lumbar vertebral bodies and intervertebral discs are automatically extracted from a mid-sagittal slice using a graphical model based approach. After that, a three-dimensional (3D) variable-radius soft tube model of the lumbar spine column is built to guide the 3D disc segmentation. The disc segmentation is achieved as a multi-kernel diffeomorphic registration between a 3D template of the disc and the observed MRI data. Experiments on 15 patient data sets showed the robustness and the accuracy of the proposed algorithm.

1 Introduction

Intervertebral disc (IVD) degeneration is a major cause for chronic back pain and function incapacity [1]. Magnetic Resonance Imaging (MRI) has become one of the key investigative tools in clinical practice to image the spine with IVD degeneration not only because MRI is non-invasive and does not use ionizing radiation, but more importantly because it offers good soft tissue contrast which allows visualization of the disc's internal structure [2].

MRI quantification has great potential as a tool for the diagnosis of disc pathology but before quantifying disc information, the IVDs need to be extracted from the MRI data. IVD extraction from MRI data comprises two key steps. Firstly, all IVDs have to be detected from the images and secondly, the regions belonging to IVDs have to be segmented. Manual extraction methods [3, 4] as well as automated extraction

X. Dong
School of Computer Science and Engineering, Southeast University, Nanjing, China
e-mail: xiao.dong@seu.edu.cn

G. Zheng (✉)
Institute for Surgical Technology and Biomechanics, University of Bern, Bern, Switzerland
e-mail: guoyan.zheng@istb.unibe.ch

J. Yao et al. (eds.), *Recent Advances in Computational Methods and Clinical Applications for Spine Imaging*, Lecture Notes in Computational Vision and Biomechanics 20, DOI 10.1007/978-3-319-14148-0_12

methods [5–11] have been presented before. Since manual extraction is a tedious and time-consuming process which lacks repeatability, automated methods are preferred.

There are different approaches for automatizing the extraction of IVDs from medical images such as graphical model [5], probabilistic model [6], Random Forest regression and classification [12, 13], watershed algorithm [7], atlas registration [8], statistic shape model [10], graph cuts [9], and anisotropic oriented flux [11]. But stable and accurate IVD segmentation remains a challenge.

In this paper we propose an automated 3D lumbar IVD extraction method with minimal user interaction from MRI data sets. The main contribution of our method is a combination of graphical model-based spine column localization with a multi-kernel diffeomorphic registration based segmentation. The 3D IVDs are extracted with a two-step procedure where we first identify the spine column structure and then carry out the IVD segmentation. The motivation behind this two-step procedure can be explained as follows. The IVD geometries are highly constrained by the geometry of the spine column. If the geometrical parameters of the spine column and each individual vertebral body can be estimated accurately from the observed images, then they can provide both geometrical and appearance information about the intervertebral discs, which helps to improve the accuracy and robustness of the IVD segmentation.

The work flow of the proposed algorithm consists of following three steps

- **Initialization**. Two user supplied landmarks are required to indicate the centers of L1 and L5 vertebral bodies.
- **Lumbar spine column identification and modeling**. Starting from the user initialization, the 3D geometry of the lumbar spine column is automatically extracted from the 3D data sets. The outputs are the 3D geometric information of each individual vertebral body of L1-L5 and a *soft-tube* model that fits the outer surface of the lumbar spine column.
- **Lumbar disc segmentation**. Based on the prior information of the extracted lumbar spine column, the disc segmentation is achieved as a multi-kernel diffeomorphic registration between a disc template and the observed data.

2 Methods

2.1 Data Sets

All datasets used in this paper were generated from a 1.5 Tesla MRI scanner (Siemens, Erlangen, Germany). Dixon protocol was used to reconstruct four aligned high-resolution 3D volumes during one data acquisition: in-phase, opposed-phase, water and fat images, as shown in Fig. 1. Each volume has a resolution of $2 \times 1.25 \times 1.25\,\text{mm}^3$ and the data set size is $40 \times 512 \times 512$. The advantage of working with such datasets is that different channels provide complementary information for our disc segmentation task. In our proposed segmentation strategy, we always first extract

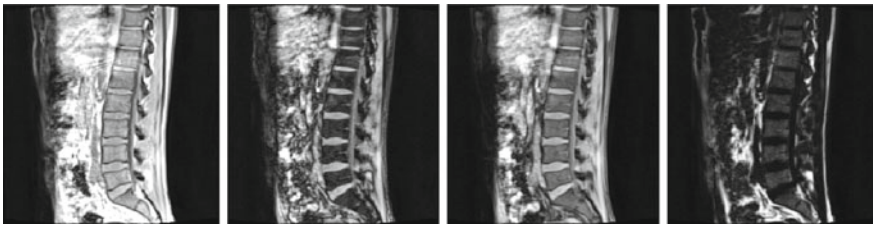

Fig. 1 The four aligned channels of a patient data (for visualization purpose, we only show the middle sagittal (mid-sagittal) slice of each channel.)

either intensity or feature information about different tissues on each channel and then combine the 4 channel data into a single dataset.

2.2 Lumbar Spine Column Identification

On the mid-sagittal slice, two landmarks are picked to indicate the centers of L1 and L5 vertebral bodies as shown in Fig. 2a. Starting from the initialization, we first carry out a 2D vertebral body and disc identification to localize vertebrae L1-L5 and the 5 target discs from the mid-sagittal slice. The geometrical information of the 2D identification is then used to guide a further 3D lumbar spine column modeling.

2.2.1 2D Vertebral Body and Disc Identification

Solutions for spine location and disc labeling include feature-based bottom-up methods, statistical model-based methods and graphical model-based solutions. For a detailed review of the existing methods, we refer to [14]. In this paper, the 2D vertebral body and disc identification is achieved using a graphical model based strategy introduced in [14]. Compared with the graphical models in [5, 6], the advantage of the graphical model in [14] is that both the low level image observation model and the high level vertebra context potentials need not to be learned from training data. Instead they are capable of self-learning from the image data during the inference procedure. For completeness, here we describe the key components of the method that we previously introduced [14].

1. **The graphical model**: The graphical model is given in Fig. 2d. Each node V_i represents a connected disc-vertebrae-disc chain of the spine, whose geometrical parameters are given by X_i. We define
   - **The component observation model**. $p(I|X_i)$ of a single component V_i representing the probability that the configuration X_i of the node V_i match the observed images I.

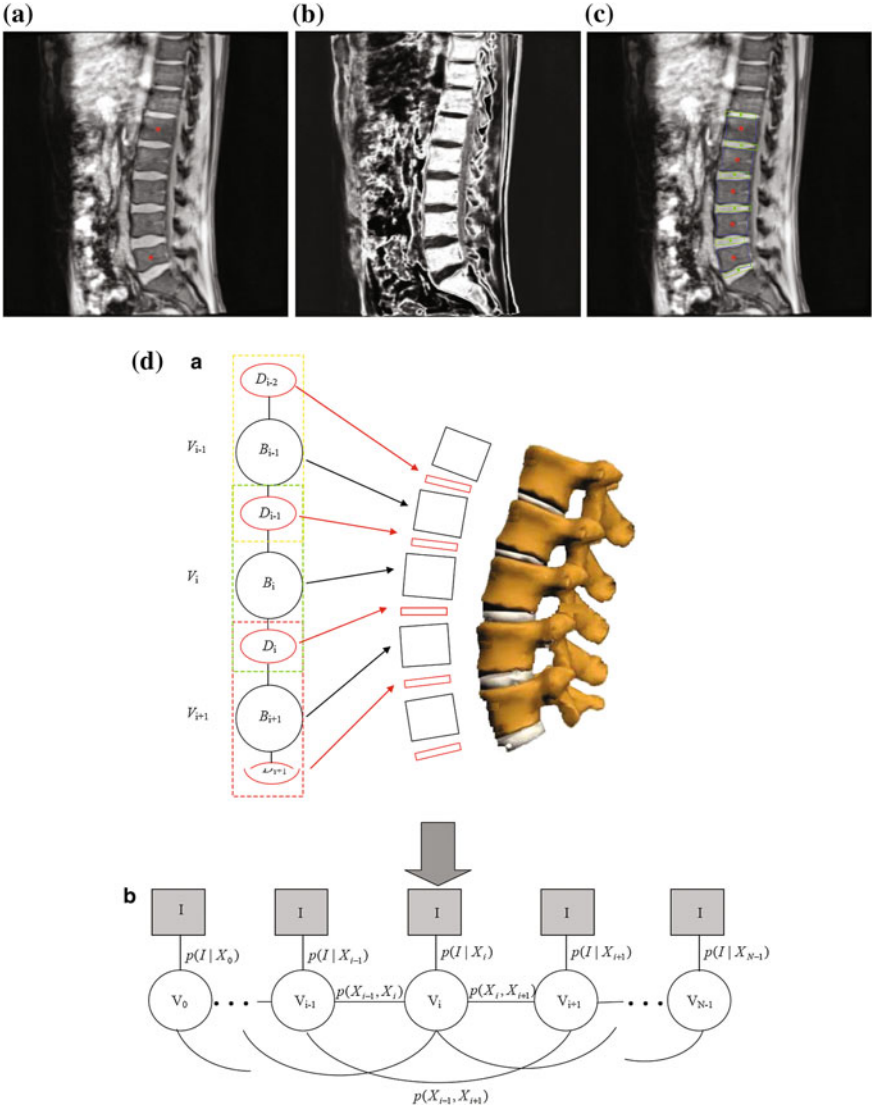

Fig. 2 Initialization and 2D lumbar spine column detection. **a** User initialization by picking two landmarks indicating the centers of L1 and L5 in the middle sagittal slice. **b** Probability assignment (displayed as grey values) of the bone tissue in the mid-sagittal slice for 2D lumbar spine column detection. **c** 2D lumbar spine column detection result using the graphical model based detection algorithm, *blue* and *green* rectangles representing the vertebral bodies and IVDs respectively. **d** Graphical model of 2D lumbar column detection (Color figure online)

- **The potentials**. $p(X_i, X_j)$ *between neighboring components* V_i and V_j encoding the geometrical constraints between components which are defined by the anatomical structure of the spine column.

The identification of the spine column from the mid-sagittal slice can then be formalized as to find the optimal configurations of $\{V_i\}$, $X = \{X_i\}$ that maximize

$$P(X|I) \propto \Pi_i p(I|X_i) \Pi_{i,j} p(X_i, X_j) \tag{1}$$

with

$$p(I|X_i) = p_I(I|X_i) p_G(I|X_i) \tag{2}$$

and

$$p(X_i, X_j) = p_S(X_i, X_j) p_O(X_i, X_j) p_D(X_i, X_j) \tag{3}$$

$p_I(I|X_i)$ and $p_G(I|X_i)$ stand for the probabilities that the observed image intensity and image gradient distributions match the geometrical parameters X_i respectively. $p_S(X_i, X_j)$, $p_O(X_i, X_j)$ and $p_D(X_i, X_j)$ are the geometrical constraints on the sizes, orientations and distances between neighboring components. All the observation models and constraints can be designed according to the observed data and prior anatomical knowledge of the spine structure. For detailed formulation of these terms, we refer to [14].

2. **Optimization**: The optimization is achieved as an inference on the graphical model. The method introduced in [14], which is a particle based nonparametric belief propagation on the graphical model, is used here to carry out the inference.

Figure 2b shows an example of the bone tissue probability assignment on the mid-sagittal slice, which is computed from the user supplied 2 landmarks (Fig. 2a) and 4 channel volume data (see Fig. 1 for an example) by a Gaussian distribution modeling and an equally weighted combination of the intensity distributions of the bony tissue in the 4 channels. This image is used for the computation of the intensity observation model $p_I(I|X_i)$ during the 2D lumbar column detection. Figure 2c gives the 2D lumbar column detection result. It can be observed that the centers, sizes and orientations of the vertebral bodies and IVDs are correctly identified.

2.2.2 3D Lumbar Spine Column Modeling

We model each lumbar vertebral body as an elliptical cylinder and the lumbar spine column as a variable-radius soft tube. Details of the modeling procedure are described as follows:

- **3D modeling of each vertebral body**: From the 2D vertebral body identification results, the position, hight, radius and orientation of each vertebral body and the image intensity distribution of the bone region can be estimated by modeling the vertebral body as a cylinder. Accordingly for each voxel in the neighbourhood of

the estimated cylinder, we can assign the probability that it belongs to the bony tissue. To refine the 3D modeling of the vertebral bodies, we then further model the vertebral body as an elliptical cylinder, a least-squares geometric fitting to the voxels assigned with a high probability (>0.8) of belonging to the bony tissue can extract the 3D geometry of each vertebral body, including the center, height, orientation and the major radius and minor radius of the elliptical cylinder model.

- **3D modeling of the spine column**: The lumbar column can be modeled as a variable-radius soft tube that contains all the extracted vertebral bodies. Given the 3D models of L1-L5 vertebral bodies, the central axis and the variable-radius of the soft tube can be obtained by a linear interpolation on the centers and radii of the extracted 3D models of vertebral bodies. This results in a 3D variable-radius soft-tube spine column model as shown in Fig. 3a.

Given the 3D soft-tube lumbar spine column model, the spine column region can be extracted from the observed data sets (Fig. 3b). By further eliminating the bony tissue region using the 3D models of vertebral bodies, the candidate region for each target disc can be localized as shown in Fig. 3c–f. The following 3D IVD segmentation is then carried out on the extracted candidate IVD regions.

2.3 3D Disc Segmentation

We solve the 3D disc segmentation as a template based registration between a geometrical disc template and the observed data.

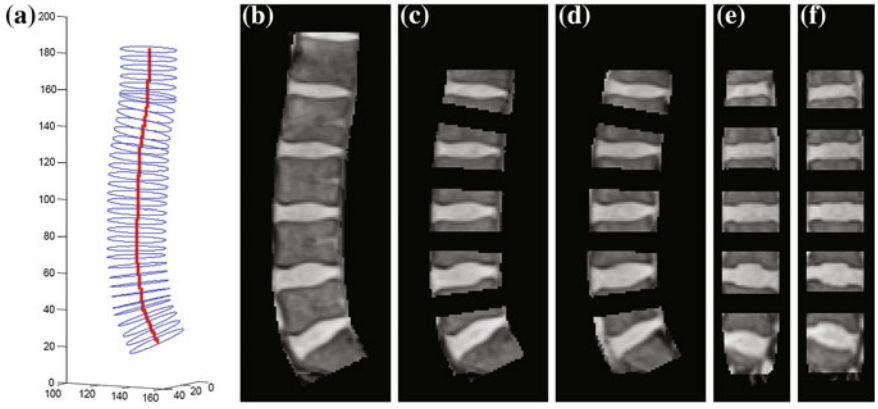

Fig. 3 3D lumbar spine column detection and modeling. **a** the 3D soft-tube model of the lumbar spine column; **b** segmented lumbar spine column image; **c–d** segmented disc candidate regions in sagittal slices; **e–f** segmented disc candidate regions in coronal slices. Although all tasks are conducted in 3D, here we show the results in 2D slices for visualization purpose

- The IVD template is set as a thin elliptical cylinder. Considering the anatomical structure of the spine column, i.e., each IVD must fall between its neighbouring vertebral bodies, the initial geometries (center, radii, orientation, hight) of the IVD cylinder template can be estimated using the 3D spine column model and the geometries of its neighboring vertebral bodies, which are all available from the previous 3D lumbar spine column modeling procedure.
- For the segmentation of a specific IVD, the correspondent observed data to be matched is just the extracted candidate IVD region as shown in Fig. 3c–f
- The registration algorithm we choose is a multi-kernel diffeomorphic image matching in the Large Deformation Diffeomorphic Metric Mapping (LDDMM) framework as described in [15] and related literatures [16–18].

2.3.1 Multi-kernel LDDMM Registration

LDDMM framework [17] is one of the two main computational frameworks in computational anatomy [16]. Existing works show that LDDMM is a general solution for nonrigid image registration with a high flexibility and accuracy. In [15] multi-kernel LDDMM registration algorithms were investigated. Compared with the LDDMM registration with a single kernel, multi-kernel LDDMM has the capability to optimize the deformation in multiple spatial scales [15].

Following the general idea of LDDMM framework, we formalize the multi-kernel image registration between two images I_0 and I_1 as an optimization problem to find the optimal time dependent velocity field $v(t)$ that minimizes the sum of a similarity and a deformation energy formalized as

$$\mathscr{E}(v^{\alpha}(t)) = \frac{1}{2}\sum_i w^i \int_0^1 \|v^i(t)\|^2_{V^i} dt + \|I_0 \circ \phi_v^{-1}(1) - I_1\|^2_{L^2} \tag{4a}$$

$$\frac{\partial}{\partial t}\phi_v(t) = v(t) \circ \phi_v(t) \tag{4b}$$

$$v(t) = \sum_i v^i(t) \tag{4c}$$

$$\phi_v(0) = Id \tag{4d}$$

where $\|v^i(t)\|_{V^i} =< v^i(t), v^i(t) >^{\frac{1}{2}}_{V^i}$ is the norm induced by the inner product $< u, v >_{V^i} =< L_{V^i}u, L_{V^i}v >_{L^2}$, and $\{K_{V^i} = (L^+_{V^i}L_{V^i})^{-1}\}$ are the kernels. The $\phi_v(t)$ is the time-dependent deformation computed as the integration of the velocity field $v(t)$ and $I_0 \circ \phi_v^{-1}(t)$ is the transformed image of I_0 by the deformation $\phi_v(t)$.

Using the optimal control based approach introduced in [19, 20], we get the Euler-Poincare equation (EPDiff) for the multi-kernel LDDMM registration algorithm as

$$\dot{I}(t) = -\nabla I(t) \cdot \sum_i v^i(t) \tag{5a}$$

$$\dot{P}(t) = -\nabla (P(t) \cdot \sum_i v^i(t)) \tag{5b}$$

$$v^i(t) = -(w^i)^{-1} K_{V^i} \star (P(t) \nabla I(t)) \tag{5c}$$

$$P(1) = -(I(1) - I_1) \tag{5d}$$

$$I(0) = I_0 \tag{5e}$$

The registration can then be carried out by updating the deformation velocity fields $v^i(t)$ iteratively from an initial value of $v^i(t)$ using Eqs. (5a)–(5e). For more details on the computation routine, we refer to [17, 19, 20].

2.3.2 Disc Segmentation by Diffeomorphic Registration

The IVD segmentation is achieved as a template based registration between the thin cylinder IVD template and the correspondent candidate disc region as shown in Fig. 3.

In order to explore both intensity and feature information to enhance the accuracy and robustness of the segmentation, we consider a simultaneous registration of two pairs of images, I_0^I / I_1^I and I_0^E / I_1^E, which stand for the image intensity and edge information template/observation pairs respectively. Accordingly in the cost function of the LDDMM registration (4a), the image similarity term includes two components $\| I_0^I \circ \phi_v^{-1}(1) - I_1^I \|_{L^2}^2 + \beta \| I_0^E \circ \phi_v^{-1}(1) - I_1^E \|_{L^2}^2$ (Fig. 4).

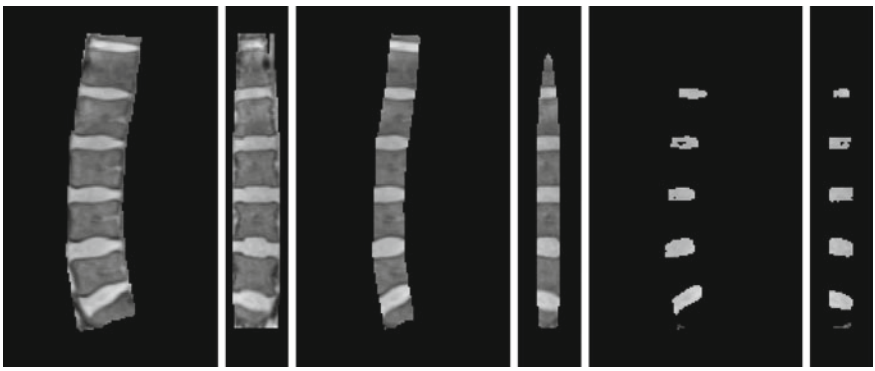

Fig. 4 Determination of the high confidence disc region using the spine column model. *Left* to *right*: The spine column region extracted using the spine column model shown in a sagittal and a coronal slice; The central region of the spine column obtained by shrinking the radius of the spine column model by a factor 0.5 shown in the same two slices; The detected high confidence disc regions by further cutting out the bone tissue using the spine column model

I_0^I / I_1^I and I_0^E / I_1^E can be computed from the initialized IVD template and the extracted IVD candidate regions. Details about how to compute them are omitted due to limited space. An example of the template images and correspondent target images and the time dependent registration procedure is shown in Fig. 5.

The final segmented IVD can then be obtained as the deformed template achieved by the multi-kernel LDDMM registration.

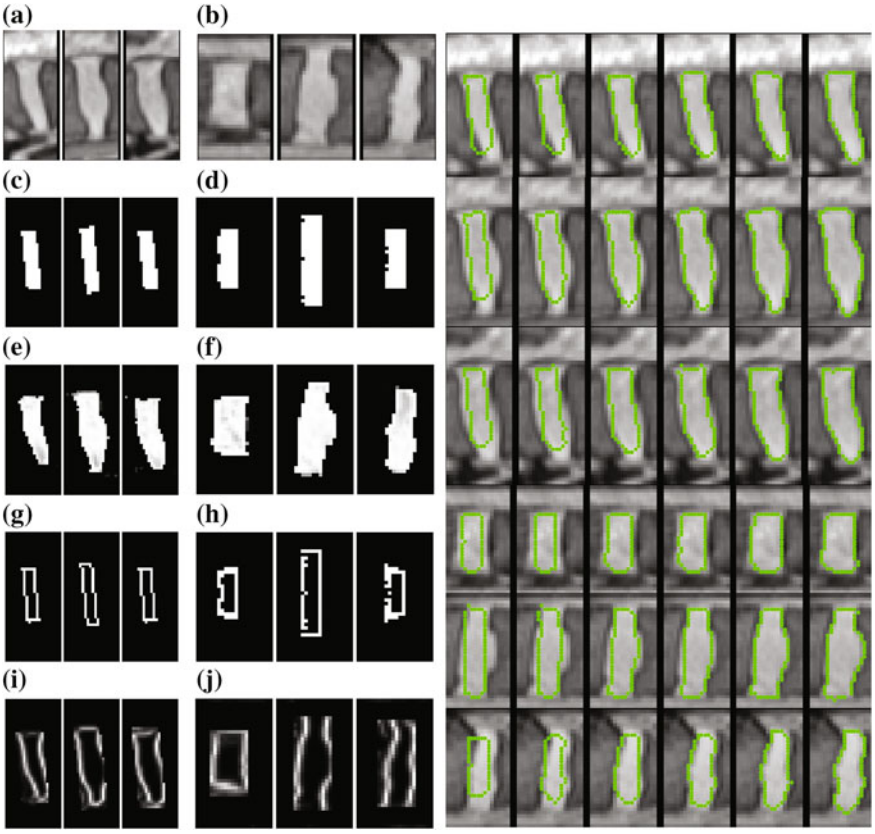

Fig. 5 3D IVD segmentation by multi-kernel LDDMM registration *Left side*: The data used in diffeomorphic registration based 3D lumbar disc segmentation. In the target images, the bone tissue regions are extracted using the spine column model. **a**–**b**: 3 sagittal/coronal slices of the candidate disc region (disc L4-L5 in Fig. 2); **c**–**d**: the intensity disc template in 3 sagittal/coronal slices; **e**–**f**: intensity information extracted from MRI data sets in 3 sagittal/coronal slices; **g**–**h**: the edge disc template in 3 sagital/coronal slices; **i**–**j**:edge information computed from MRI data sets in 3 sagittal/coronal slices; *Right side*: The time-dependent deformation of the disc template during the multi-kernel diffeomorphic registration for a L4-L5 disc segmentation. *left* to *right*: the deformations of the template at 6 time slots $t = 0, 0.2, 0.4, 0.6, 0.8, 1$. $t = 0$ means the initial template and $t = 1$ gives the final registration results; from *top row* to *bottom row*: the evolution of the template visualized in 6 different slices

3 Experiments

The proposed algorithms are verified on MRI datasets of 15 patients obtained with the Dixon protocol. In all the data sets, based on the two landmarks obtained from the initialization step, both the 2D lumbar spine column and the 3D spine column models are correctly extracted. Examples of the disc segmentation results on 4 patient data sets are shown in Fig. 6.

We also carried out quantitative evaluation of our algorithm. To do this, we manually segmented all datasets (we only need to segment one channel for each patient as all four channel volumes are aligned according to Dixon imaging protocol) and took the binary volumes from the manual segmentation as the ground truth to verify the accuracy of the present algorithm. We computed the Dice coefficient D which is usually used to measure the overlap between two binary images:

$$D = \frac{2 \times |A \cap B|}{|A| + |B|} \times 100 \tag{6}$$

Table 1 shows the average dice coefficients of the 5 discs on all 15 patients when the automated segmentation was compared to the manual segmentation. The highest average dice coefficient was found for patient #8 (87.9 %) and the lowest average dice coefficient was found for patient #9 (80.5 %). We also computed the average

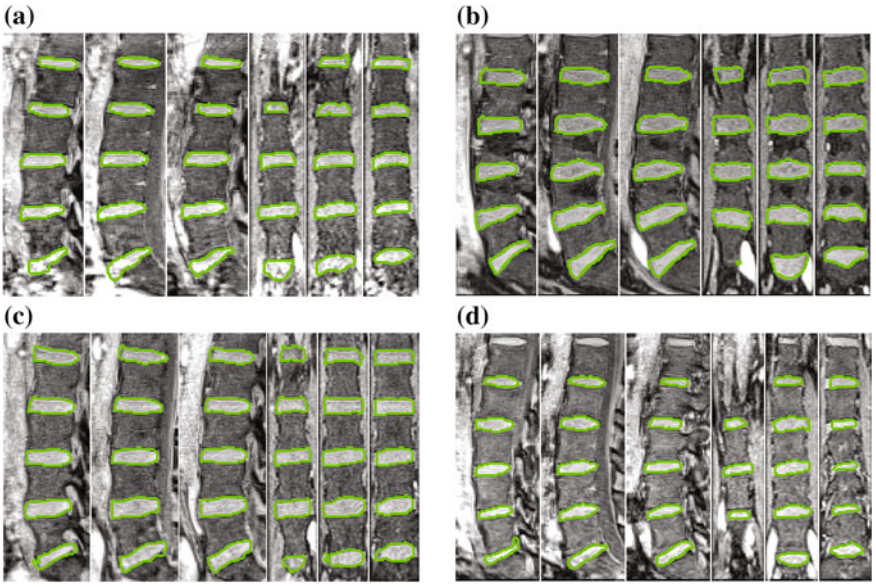

Fig. 6 3D intervertebral disc segmentation results on 4 patients. For visualization purpose, we display the results on 2D slices. For each image, the left three columns are sagittal slices and the right three are coronal slices

Table 1 Average Dice coefficients (%) of the 5 discs between the manual segmentation and the proposed algorithm on different patients

Patient	P1	P2	P3	P4	P5	P6	P7	P8	P9	P10	P11	P12	P13	P14	P15
Dice	86.1	81.9	82.6	86.3	86.8	83.6	87.6	87.9	80.5	84.1	86.3	85.4	86.9	87.7	83.1

Table 2 Average Dice coefficients (%) between the manual segmentation and the proposed algorithm on different discs on all 15 data sets

Disc	L1-L2	L2-L3	L3-L4	L4-L5	L5-S1
Dice	81.2	87.1	88.2	86.5	82.7

dice coefficients for all discs and the results are presented in Table 2. We note that Neubert et al. [10] reported a mean Dice of 76–80 % in their 3D IVD segmentation paper.

4 Conclusions

In this paper we proposed an automated lumbar intervertebral disc segmentation strategy, whose key components include a graphical model based spine column identification algorithm and a multi-kernel LDDMM registration algorithm to achieve the disc segmentation. By identifying the lumbar spine column structure before carrying out the segmentation, we acquire geometrical and appearance information about the spine column. These information can be used to accurately locate the candidate disc region and provide constraints to enhance the performance of the disc segmentation. By converting the segmentation problem as a template based diffeomorphic registration, we can explore both the intensity and edge information of the observed data while keeping a smooth deformation of the template so that the final segmented discs will possess smooth surfaces. The experiments on 15 patient data sets verified the robustness and accuracy of our method.

We also noticed that for abnormal cases, such as with missing/additional vertebrae or the scoliosis case, the automated lumbar column identification may not be reliable although the graphical model can handle the unknown vertebra number as shown in [14]. A possible solution for these extreme cases is to ask the user to indicate the center of each vertebra body during the initialization step. Once the centers are known, the particle filtering-based inference can then achieve a reliable 2D lumbar column identification and the following up 3D lumbar column modeling and disc segmentation.

References

1. Modic, M., Ross, J.: Lumbar degenerative disk disease. Radiology **245**(1), 43–61 (2007)
2. Parizel, P., Goethem, J.V., den Hauwe, L.V., Voormolen, M.: Degenerative disc disease. In: Van Goethem, J. (ed.) Spinal Imaging—Diagnostic imaging of the spine and spinal cord, pp. 122–133. Springer, Berlin (2007)
3. Tsai, M., Jou, J., Hsieh, M.: A new method for lumbar herniated intervertebral disc diagnosis based on image analysis of transverse sections. Comput. Med. Imaging Graph. **26**(6), 369–380 (2002)
4. Niemelainen, R., Videman, T., Dhillon, S., Battie, M.: Quantitative measurement of intervertebral disc signal using mri. Clin. Radiol. **63**(3), 252–255 (2008)
5. Schmidt, S., Kappes, J.H., Bergtholdt, M., Pekar, V., Dries, S., Bystrov, D., Schnorr, C.: Spine detection and labeling using a parts-based graphical model. In: N. Karssemeijer, B.L. (ed.) IPMI, pp. 122–133. Springer, Berlin (2007)
6. Corso, J., Alomari, R., Chaudhary, V.: Lumbar disc localization and labeling with a probabilistic model on both pixel and object features. In: Metaxas, e.a., D. (ed.) MICCAI, pp. 202–210. Springer, Berlin (2008)
7. Chevrefils, C., Cheriet, F., Aubin, C., Grimard, G.: Texture analysis for automatic segmentation of intervertebral disks of scoliotic spines from mr images. IEEE Trans. Inf. Technol. Biomed. **13**(4), 608–620 (2009)
8. Michopoulou, S., Costaridou, L., Panagiotopoulos, E., Speller, R., Panayiotakis, G., Todd-Pokropek, A.: Atlas-based segmentation of degenerated lumbar intervertebral discs from mr images of the spine. IEEE Trans. Biomed. Eng. **56**(9), 2225–2231 (2009)
9. Ayed, I.B., Punithakumar, K., Garvin, G., Romano, W., Li, S.: Graph cuts with invariant object-interaction priors: application to intervertebral disc segmentation. In: G. Szekely, H.H. (ed.) IPMI, pp. 221–232. Springer, Berlin (2011)
10. Neubert, A., Fripp, J., Schwarz, R., Lauer, L., Salvado, O., Crozier, S.: Automated detection, 3d segmentation and analysis of high resolution spine mr images using statistical shape models. Phys. Med. Biol. **57**, 8357–8376 (2012)
11. Law, M., Tay, K., Leung, A., Garvin, G., Li, S.: Intervertebral disc segmentation in mr images using anisotropic oriented flux. Med. Image Anal. **17**(1), 43–61 (2013)
12. Glocker, B., Feulner, J., Criminisi, A., Haynor, D., Konukoglu, E.: Automatic localization and identification of vertebrae in arbitrary field-of-view ct scans. MICCAI, pp. 590–598. Springer-Verlag, Berlin (2012)
13. Glocker, B., Zikic, D., Konukoglu, E., Haynor, D., Criminisi, A.: Vertebrae localization in pathological spine ct via dense classification from sparse annotations. MICCAI, pp. 262–270. Springer, Berlin (2013)
14. Dong, X., Lu, H., Sakurai, Y., Yamagata, H., Zheng, G., Reyes, M.: Automated intervertebral disc detection from low resolution, sparse mri images for the planning of scan geometries. In: Wang, F., Yan, P., Suzuki, K., Shen, D. (eds.) Machine Learning Medical Imaging. Lecture Notes in Computer Science, pp. 10–17. Springer, Berlin Heidelberg (2010)
15. Risser, L., Vialard, F.X., Wolz, R., Murgasova, M., Holm, D.D., Rueckert, D.: Simultaneous multiscale registration using large deformation diffeomorphic metric mapping. IEEE Trans. Med. Imaging **30**(10), 1746–1759 (2011)
16. Grenander, U., Miller, M.I.: Computational anatomy: An emerging discipline. Quarterly of Applied Mathematics LVI(4), pp. 617–694. (1998)
17. Beg, M.F., Miller, M.I., Trouv, A., Younes, L.: Computing large deformation metric mappings via geodesic flow of diffeomorphisms. Int. J. Comput. Vis. **61**, 139–157 (2005)
18. Miller, M.I., Trouv, A., Younes, L.: Geodesic shooting for computational anatomy. J. Math. Imaging. Vis. **24**(2), 209–228 (2006)
19. Hart, G.L., Zach, C., Niethammer, M.: An optimal control approach for deformable registration. In: Computer Vision and Pattern Recognition. (2009)
20. Vialard, F.X., Risser, L., Rueckert, D., Cotter, C.J.: Diffeomorphic 3d image registration via geodesic shooting using an efficient adjoint calculation. Int. J. Comput. Vis. **97**, 229–241 (2012)